

AD-A056 958

AIR FORCE GEOPHYSICS LAB HANSCOM AFB MASS

F/G 4/2

CALCULATION OF THE BUOYANT MOTION OF A TURBULENT PLANAR HEATED --ETC(U)

MAR 78 M M KLEIN

UNCLASSIFIED

AFGL-TR-78-0072

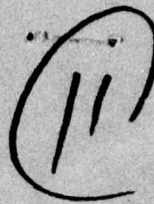
NL

| OF |
AD
A056958



END
DATE
FILMED
9 -78
DDC

LEVEL II



2

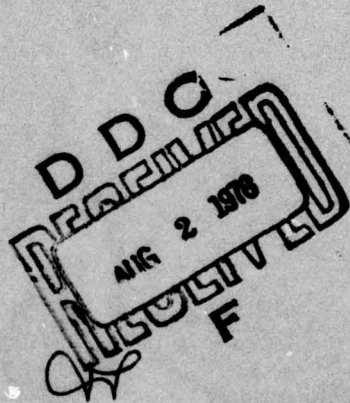
AFGL-TR-78-0072
AIR FORCE SURVEYS IN GEOPHYSICS, NO. 385



AD A 056958

**Calculation of the Buoyant Motion
of a Turbulent Planar Heated Jet
in an Opposing Air Stream**

MILTON M. KLEIN



AD No. [unclear]
DDC FILE COPY

23 MARCH 1978

Approved for public release; distribution unlimited.

METEOROLOGY DIVISION PROJECT 2093
AIR FORCE GEOPHYSICS LABORATORY
HANSCOM AFB, MASSACHUSETTS 01731

AIR FORCE SYSTEMS COMMAND, USAF

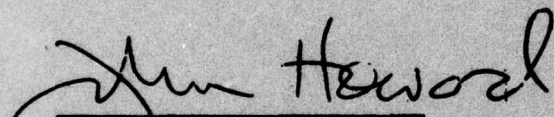


78 07 31 154

This report has been reviewed by the ESD Information Office (OI) and is releasable to the National Technical Information Service (NTIS).

This technical report has been reviewed and is approved for publication.

FOR THE COMMANDER



Chief Scientist

Qualified requestors may obtain additional copies from the Defense Documentation Center. All others should apply to the National Technical Information Service.

Unclassified

SECURITY CLASSIFICATION OF THIS PAGE (When Data Entered)

REPORT DOCUMENTATION PAGE		READ INSTRUCTIONS BEFORE COMPLETING FORM
1. REPORT NUMBER AFGL-TR-78-0072, AFGL-AFSG-385	2. GOVT ACCESSION NO.	3. SCIENTIFIC CATALOG NUMBER
4. TITLE (and Subtitle) CALCULATION OF THE BUOYANT MOTION OF A TURBULENT PLANAR HEATED JET IN AN OPPOSING AIR STREAM	5. TYPE OF REPORT & PERIOD COVERED Scientific. Interim.	
7. AUTHOR(s) Milton M. Klein	6. PERFORMING ORG. REPORT NUMBER AFSG No. 385	
9. PERFORMING ORGANIZATION NAME AND ADDRESS Air Force Geophysics Laboratory (LYP) Hanscom AFB Massachusetts 01731	10. PROGRAM ELEMENT, PROJECT, TASK AREA & WORK UNIT NUMBERS 62101F 2093 17 01	
11. CONTROLLING OFFICE NAME AND ADDRESS Air Force Geophysics Laboratory (LYP) Hanscom AFB Massachusetts 01731	12. REPORT DATE 23 Mar 1978	
14. MONITORING AGENCY NAME & ADDRESS (if different from Controlling Office)	13. NUMBER OF PAGES 34	
	15. SECURITY CLASS. (of this report) Unclassified	
16. DISTRIBUTION STATEMENT (of this Report) Approved for public release; distribution unlimited.		
17. DISTRIBUTION STATEMENT (of the abstract entered in Block 20, if different from Report)		
18. SUPPLEMENTARY NOTES		
19. KEY WORDS (Continue on reverse side if necessary and identify by block number) Thermal fog dispersion Buoyancy Counterflowing jet Turbulence Heated jet Planar jet		
20. ABSTRACT (Continue on reverse side if necessary and identify by block number) A broad experimental and theoretical program is being conducted to aid in the development of an operational warm fog dispersal system which utilizes momentum driven ground based heat sources. To help determine optimum heat and thrust combinations for the system, investigations are being made of the buoyant motion of heated turbulent jets both coflowing (wind and jet in the same direction) and counterflowing (wind and jet opposite). The investigation of the coflowing jet has been completed and in addition a model has been developed.		

Air Force surveys in geophysics

next page

DD FORM 1 JAN 73 1473 EDITION OF 1 NOV 65 IS OBSOLETE

Unclassified

SECURITY CLASSIFICATION OF THIS PAGE (When Data Entered)

449 578

78 07 31 154

hc

Unclassified

SECURITY CLASSIFICATION OF THIS PAGE(When Data Entered)

20. Abstract (Continued)

from which the dynamic characteristics of a heated counterflowing jet in the absence of buoyancy can be calculated. The present investigation is concerned with the effect of buoyancy upon the motion of a counterflowing jet.

The lower portion of the trajectory, which has been calculated by the present model, is in fair to good agreement with the corresponding experimental curve, the calculated curve tending to be somewhat higher than that obtained experimentally. The calculated upper part of the trajectory, obtained from a model which gives the deflection of a jet in a crosswind, is in good agreement with experiment.

The present model yields a scaling law for a counterflowing jet which indicates that the scaling depends principally upon the Froude number defined by the initial jet velocity and excess temperature and very weakly upon the initial jet temperature. This result is essentially the same as that obtained for the coflowing jet for the case of small values of windspeed relative to initial jet velocity.

Unclassified

SECURITY CLASSIFICATION OF THIS PAGE(When Data Entered)

Preface

The author would like to thank Mr. Bruce A. Kunkel for his critical review and constructive criticism of the final manuscript.

ACCESSION for	
NTIS	White Section <input checked="" type="checkbox"/>
DDC	Buff Section <input type="checkbox"/>
UNANNOUNCED	<input type="checkbox"/>
JUSTIFICATION	
BY	
DISTRIBUTION/AVAILABILITY CODES	
Dist.	of SPECIAL
A	

Contents

1. INTRODUCTION	7
2. JET GEOMETRY	8
3. ANALYSIS FOR ZONE I	10
3.1 Axial Distributions for Counterflowing Jet	10
3.2 Calculation of the Buoyant Force	12
3.3 Trajectory Analysis	14
3.4 Dependence of Vertical Velocity and Trajectory Upon Parameters	18
3.5 Scaling Law for Counterflowing Jet	19
4. ANALYSIS FOR ZONE II	19
4.1 Axial Distributions	19
4.2 Determination of the Buoyant Force	20
4.3 Calculation of the Trajectory	21
5. CALCULATION OF UPPER PORTION OF TRAJECTORY	23
6. DETERMINATION OF LIFT-OFF POINT AND LENGTH OF JET FROM EXPERIMENTAL DATA	24
7. RESULTS AND DISCUSSION	26
8. SUMMARY AND CONCLUSIONS	30
REFERENCES	31
LIST OF SYMBOLS	33

Illustrations

1a. Schematic Representation of Geometry of Counterflowing Jet and Velocity and Temperature Profiles	9
1b. Schematic Representation of Jet Centerline Trajectory	9
2. Plot of Experimental Values of Lift-off Point x_0 Against Parameter p ; Solid Curve is Power Law Fit to Experimental Points	25
3. Plot of Experimental Values of Jet Length x_2 Against Parameter p ; Solid Curve is Power Law Fit to Experimental Points	26
4. Comparison of Calculated Trajectories, for Several Tests, With Corresponding Experimental Curves, Test 3-4	27
5. Comparison of Calculated Trajectories, for Several Tests, With Corresponding Experimental Curves, Test 4-4	27
6. Comparison of Calculated Trajectories, for Several Tests, With Corresponding Experimental Curves, Test 5-4	28
7. Comparison of Calculated Trajectories, for Several Tests, With Corresponding Experimental Curves, Test 5-19	28
8. Comparison of Calculated Trajectories, for Several Tests, With Corresponding Experimental Curves, Test 6-2	29
9. Comparison of Calculated Trajectories, for Several Tests, With Corresponding Experimental Curves, Test 8-10A	29

Calculation of the Buoyant Motion of a Turbulent Planar Heated Jet in an Opposing Air Stream

1. INTRODUCTION

As part of the development of an operational Warm Fog Dispersal System (WFDS), experimental and theoretical studies have been made of the characteristics of ground based heated jets for various combinations of heat and thrust under different wind conditions. The dynamic characteristics of a nonbuoyant coflowing jet, that is, jet in the same direction as the wind, are well known and presented in detail by Abramovich.¹ The method of calculating the buoyant motion of a heated submerged jet, that is, no wind, (Abramovich²) can be extended in a straightforward manner to the case of the coflowing jet, planar or round (Klein and Kunkel^{3,4}). For simplicity, the attachment of the jet to the ground (ground effect) was neglected in

(Received for publication 22 March 1978)

1. Abramovich, G. N. (1963) The Theory of Turbulent Jets, The MIT Press, Cambridge, Mass., Chapters 4 and 5.
2. Abramovich, G. N. (1963) The Theory of Turbulent Jets, The MIT Press, Cambridge, Mass., Chapter 12, pp 580-585.
3. Klein, M. M., and Kunkel, B. A. (1975) Interaction of a Buoyant Turbulent Planar Jet With a Coflowing Wind, AFCRL-TR-75-0368.
4. Klein, M. M., and Kunkel, B. A. (1975) Interaction of a Buoyant Turbulent Round Jet With a Coflowing Wind, AFCRL-TR-75-0581.

these investigations. A method of taking into account the ground effect for a coflowing jet has been developed by Klein.⁵

The situation for the nonbuoyant counterflowing jet, that is, jet and wind directions opposite, as presented by Abramovich,⁶ is considerably less satisfactory both with regard to theory and experiment. Here the calculations, which must account for the regions of counterflow, are quite specialized and not easily adapted to the buoyant jet. Recently, however, a simplified model for a counterflowing round jet has been developed by Sekundov,⁷ which may be extended in a straightforward manner to take account of buoyancy and obtain the jet trajectories. An important feature of the Sekundov model is the use of a finite wall to help simplify the equations of motion. The results for an open jet are then obtained by making the wall arbitrarily large. The Sekundov model, which is limited to the case of an unheated incompressible jet, has been extended to take account of heat addition and density variation, while neglecting the buoyant motion (Klein⁸). The present investigation is concerned with the buoyant motion of the counterflowing jet. Since the jets in the warm fog dispersal system merge a short distance downstream of the jet nozzles,⁹ the investigation, parallel to that reference 8, has been confined to the planar case.

As in the case of the coflowing jet, experiments⁹ show that the counterflowing jet also remains attached to the ground for some distance downstream of the nozzle, resulting in a delayed lift-off point. A method of analysis similar to that of reference 5 was utilized to determine the point of lift-off.

2. JET GEOMETRY

A schematic sketch of the flow pattern for a planar jet is shown in Figure 1a while the corresponding trajectory of the jet centerline is given in Figure 1b. Here u and T denote velocity and temperature, while the subscripts o , m and a designate initial, axial and ambient values. In the initial section, where the

5. Klein, M. M. (1977) A Method for Determining the Point of Lift-Off and Modified Trajectory of a Ground-Based Heated Turbulent Planar Jet in a Coflowing Wind, AFGL-TR-77-0033.
6. Abramovich, G. N. (1963) The Theory of Turbulent Jets, The MIT Press, Cambridge, Mass., Chapters 4 and 9.
7. Sekundov, A. N. (1969) The Propagation of a Turbulent Jet in an Opposing Stream, in Turbulent Jets of Air, Plasma and Real Gas, Consultants Bureau, New York.
8. Klein, M. M. (1977) Interaction of a Turbulent Planar Heated Jet With a Counterflowing Wind, AFGL-TR-77-0214.
9. Kunkel, B. A. (1975) Heat and Thrust Requirements of a Thermal Fog Dispersal System, AFCRL-TR-75-0472.

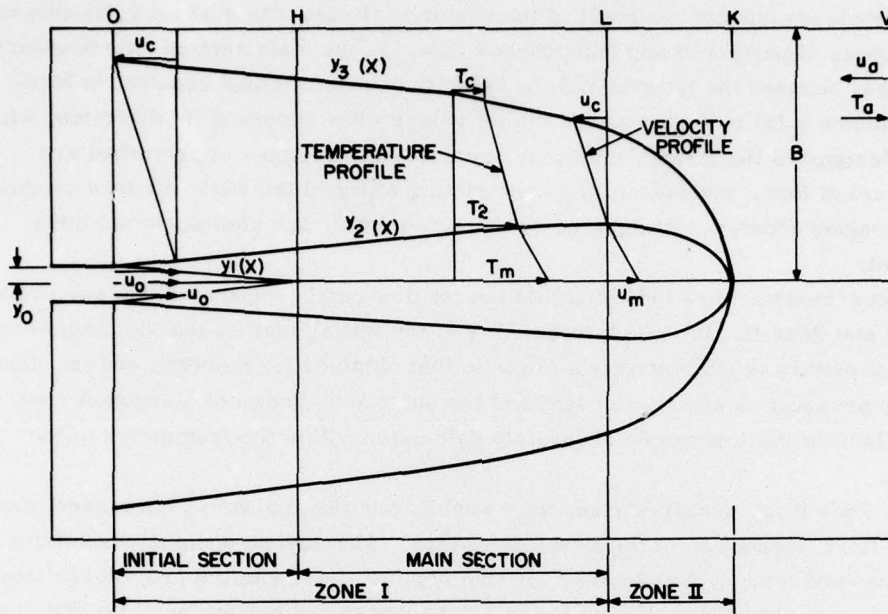


Figure 1a. Schematic Representation of Geometry of Counterflowing Jet and Velocity and Temperature Profiles

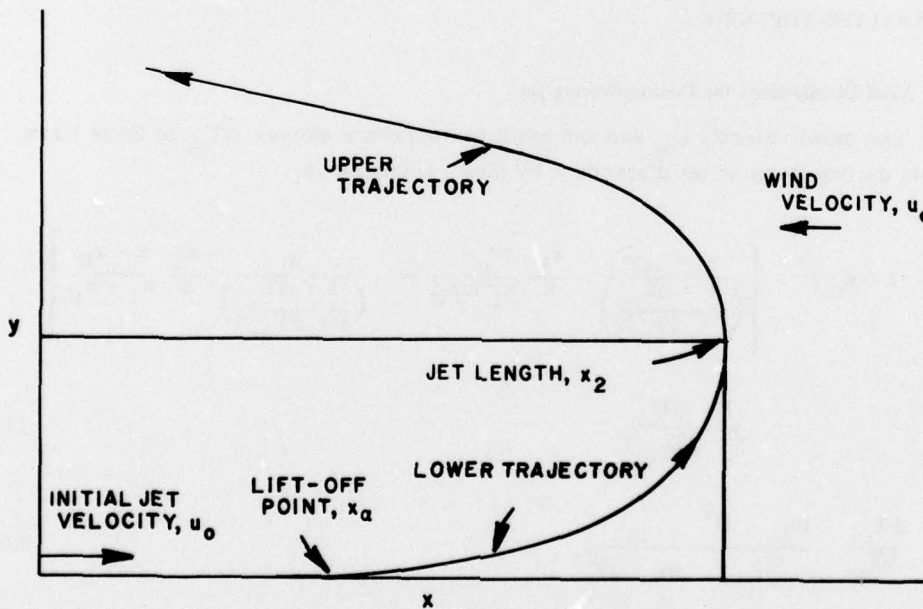


Figure 1b. Schematic Representation of Jet Centerline Trajectory

boundary layer has not yet reached the center of the jet, the surface $y_1(x)$ separates the regions of perturbed and unperturbed flow. In the main section the boundary layer has reached the jet axis and the velocity profile remains constant in form. The surface $y_2(x)$ indicates where the jet velocity has reversed its direction, while $y_3(x)$ designates the streamline which separates the regimes of perturbed and unperturbed flow. Because of the constricting effect of the walls the flow conditions in the region above y_3 , designated by the subscript c, are almost but not quite ambient.

Experimental work indicates that the jet flow can be separated into two regimes, Zone I and Zone II. In Zone I, consisting of the initial section and the main section, the flow pattern is qualitatively similar to that obtained for a submerged jet, that is, the pressure is almost constant and the surface y_2 grows at a constant rate. Here the flow pattern can be accurately calculated within the framework of the model.

In Zone II the pressure rises very rapidly and the surface y_2 decreases to zero as the final retardation of the flow takes place. Although an accurate evaluation of the flow conditions is not possible for this regime, interpolative procedures may be used since the extent of Zone II can be calculated and conditions at its end are known.

3. ANALYSIS FOR ZONE I

3.1 Axial Distributions for Counterflowing Jet

The axial velocity u_m and the axial temperature excess ΔT_m in Zone I are given as functions of jet distance x by (see reference 8)

$$(1 + u_m)^2 = \left[\frac{(1+m)^2}{\left(\frac{1+\Delta T_o}{1+\Delta T_o/2}\right)} \frac{x_H}{x} \frac{x_1-x}{x_1-x_H} + \frac{4}{\left(\frac{1+\Delta T_1}{1+\Delta T_1/2}\right)} \frac{x_1}{x} \frac{x-x_H}{x_1-x_H} \right] \frac{1+\Delta T_m}{1+\Delta T_m/2} \quad (1)$$

$$\frac{\Delta T_m}{\Delta T_o} = \frac{(u_m + 1)^2}{u_m} \frac{m}{(m+1)^2} \quad (2)$$

where ΔT_m is the temperature excess over ambient, m is the dimensionless value of the initial jet velocity u_0 referred to ambient, and the subscripts H and 1 refer to the ends of the initial and main sections. As in reference 8, velocity, density, temperature and length are taken as dimensionless, referring to initial jet half width y_0 for length and to ambient values for the other quantities.

The analysis presented in reference 8 shows that the temperature variation given by Eq. (2) is somewhat slower in the outer region of the jet than that given by experiment. We shall, therefore, utilize in place of Eq. (2) the linear form

$$\frac{\Delta T_m}{\Delta T_0} = \frac{1 + u_m}{1 + m} \quad (3)$$

which is close to Eq. (2) in the initial region of the jet but gives a slightly greater decrease in ΔT_m in the outer region.

The surface of zero velocity, $y_2(x)$, and the outer boundary of the jet, $y_3(x)$, are obtained from

$$y_2 = cx \quad (4)$$

$$N - 1 = \frac{a_1}{a_0} \rho_m u_m (2u_m + 3) \quad (5)$$

$$a_1 = \frac{1}{2} \left(1 + \frac{\rho_2}{\rho_m} \right) = \frac{1}{2} \left(1 + \frac{1 + \Delta T_m}{1 + \Delta T_2} \right) \quad (6)$$

$$a_0 = \frac{1}{2} (1 + \rho_2) = \frac{1}{2} \left(1 + \frac{1}{1 + \Delta T_2} \right) \quad (7)$$

$$\Delta T_2 = \frac{\Delta T_m}{1 + u_m} \quad (8)$$

where $N = \frac{y_3}{y_2}$, c is a growth or mixing coefficient having the value 0.22 for the main region, ρ is density, and the subscript 2 indicates values at the surface y_2 . Because of the delayed lift-off point and the initial rapid decrease in temperature, the quantities ΔT_m and ΔT_2 are small compared to unity. It will, therefore, be convenient to develop a_1 , a_0 and ρ_m to 2nd order in ΔT_m to yield

$$a_1 = 1 + \frac{v-1}{2v} \Delta T_m - \frac{(v-1)}{2v^2} \Delta T_m^2 \quad (9)$$

$$a_o = 1 + \frac{1}{2v} \Delta T_m - \frac{1}{2v^2} \Delta T_m^2 \quad (10)$$

$$\rho_m = 1 - \Delta T_m + \Delta T_m^2 \quad (11)$$

$$N - 1 = (2v + 1)(v - 1) \left[1 - \frac{\Delta T_m}{2} + \frac{(v - \frac{1}{2})}{2v} \Delta T_m^2 \right] \quad (12)$$

where $v = 1 + u_m$.

3.2 Calculation of the Buoyant Force

The buoyant force per unit length, B , is obtained from

$$B = 2g\rho_a y_o^2 \left[\int_0^{y_2} (1 - \rho) dy + \int_{y_2}^{y_3} (1 - \rho) dy \right] \quad (13)$$

where y is the vertical coordinate. In view of the small variation of pressure in the main region we may write

$$\rho = \frac{1}{T} = \frac{1}{1 + \Delta T} \quad (14)$$

and express Eq. (13) as

$$B = 2g\rho_a y_o^2 \left[\int_0^{y_2} \frac{\Delta T}{1 + \Delta T} dy + \int_{y_2}^{y_3} \frac{\Delta T}{1 + \Delta T} dy \right] \quad (15)$$

Since ΔT is small compared to unity at and beyond the lift-off point, we may develop the integrand in Eq. (15) as a power series in ΔT to yield

$$B = 2g\rho_a y_o^2 (I_1 + I_2) \quad (16)$$

$$I_1 = \int_0^{y_2} \Delta T (1 - \Delta T + \Delta T^2 - \Delta T^3 + \dots) dy \quad (17)$$

$$I_2 = \int_{y_2}^{y_3} \Delta T(1 - \Delta T + \Delta T^2 - \Delta T^3 + \dots) dy \quad (18)$$

To evaluate I_1 and I_2 , and for subsequent analysis, we require the velocity and temperature profiles. Utilizing the linear profiles of reference 8, for the region $0 \leq y \leq y_2$:

$$\frac{u}{u_m} = 1 - \frac{y}{y_2} \quad (19)$$

$$\frac{\Delta T}{\Delta T_m} = \frac{u+1}{u_m+1} = 1 - \frac{y}{ay_2} \quad (20)$$

$$a = 1 + \frac{1}{u_m}$$

$$\frac{\Delta T_2}{\Delta T_m} = \frac{1}{1+u_m} \quad (21)$$

For the region $y_2 \leq y \leq y_3$:

$$u = \frac{y - y_2}{y_3 - y_2} \quad (22)$$

$$\frac{\Delta T}{\Delta T_2} = 1 - u = 1 - \frac{y - y_2}{y_3 - y_2} \quad (23)$$

we obtain for I_1 and I_2 ,

$$I_1 = y_2 \Delta T_m \left[1 - \frac{1}{2a} - \Delta T_m \left(1 - \frac{1}{a} + \frac{1}{3a^2} \right) + \Delta T_m^2 \left(1 - \frac{3}{2a} + \frac{1}{a^2} - \frac{1}{4a^3} \right) \right] \quad (24)$$

$$I_2 = y_2(N-1) \frac{\Delta T_2}{2} \left(1 - \frac{2}{3} \Delta T_2 + \frac{\Delta T_2^2}{2} \right) \quad (25)$$

Employing Eqs. (8) and (12) for ΔT_2 and $N - 1$, and expressing a in terms of v by

$$a = \frac{1}{1 - \frac{1}{v}} \quad (26)$$

allows us to write Eqs. (24) and (25) in the form

$$I_1 = y_2 \Delta T_m \left[\frac{1}{2} \left(1 + \frac{1}{v} \right) - \frac{\Delta T_m}{3} \left(1 + \frac{1}{v} + \frac{1}{v^2} \right) + \frac{\Delta T_m^2}{4} \left(1 + \frac{1}{v} + \frac{1}{v^2} + \frac{1}{v^3} \right) \right] \quad (27)$$

$$I_2 = y_2 \Delta T_m \left(v - \frac{1}{2} - \frac{1}{2v} \right) \left[1 - \frac{\Delta T_m}{2} \left(1 + \frac{4}{3v} \right) + \Delta T_m^2 \left(1 + \frac{1}{12v} + \frac{1}{2v^2} \right) \right] \quad (28)$$

Addition of Eqs. (27) and (28) then yields for the buoyant force in Zone I.

$$B = 2 g \rho_a y_o^2 y_2 \left[v \Delta T_m - \left(\frac{v}{2} + \frac{3}{4} - \frac{1}{4v} \right) \Delta T_m^2 + \left(\frac{v}{2} + \frac{1}{12} + \frac{11}{24v} - \frac{1}{24v^2} \right) \Delta T_m^3 \right] \quad (29)$$

3.3 Trajectory Analysis

The vertical velocity is determined from the equation

$$\frac{d}{dx}(\phi V) = B \quad (30)$$

where ϕ is the mass flux through the cross section of the boundary layer and given by

$$\phi = \phi_1 + \phi_2 \quad (31)$$

with ϕ_1 the mass flux through that portion of the boundary layer below y_2 and ϕ_2 the mass flux through the part above y_2 . We note that, although ϕ_1 and ϕ_2 are in opposite directions, ϕ is given by the numerical sum of ϕ_1 and ϕ_2 . This is due to the fact that the equation for the vertical velocity is unaffected by a change in direction of the flux, that is, the vertical velocity increases positively to the right in either case.

The quantities ϕ_1 and ϕ_2 are obtained from

$$\phi_1 = 2\rho_a u_a y_o \int_0^{y_2} \rho u dy$$

$$\phi_1 = \rho_a u_a a_1 \rho_m u_m y_2 y_o \quad (32)$$

$$\phi_2 = 2\rho_a u_a y_o \int_{y_2}^{y_3} \rho u dy$$

$$\phi_2 = \rho_a u_a a_o (N - 1) y_2 y_o = \rho_a u_a a_1 \rho_m u_m (2u_m + 3) y_2 y_o \quad (33)$$

$$\phi = 2\rho_a u_a a_1 \rho_m u_m (2 + u_m) y_2 y_o \quad (34)$$

in which we have used Eq. (5) for $N - 1$.

The slope of the center line of the jet is given by

$$\frac{dy}{dx} = \frac{\phi V}{P} \quad (35)$$

where P is the momentum flux through the boundary layer and, analogous to the mass flux ϕ , given by

$$P = P_1 + P_2 \quad (36)$$

$$P_1 = 2\rho_a u_a^2 y_o \int_0^{y_2} \rho u^2 dy$$

$$P_1 = \frac{2}{3} \rho_a u_a^2 a_1 \rho_m u_m^2 y_2 y_o \quad (37)$$

$$P_2 = 2\rho_a u_a^2 y_o \int_{y_2}^{y_3} \rho u^2 dy$$

$$P_2 = \frac{2}{3} \rho_a u_a^2 a_o (N - 1) y_2 y_o = \frac{2}{3} \rho_a u_a^2 a_1 \rho_m u_m (2u_m + 3) y_2 y_o \quad (38)$$

$$P = 2\rho_a u_a^2 a_1 \rho_m u_m (u_m + 1) \quad (39)$$

Since the point of lift-off x_α is well downstream of the nozzle, the axial velocity and temperature have dropped considerably below their initial values and vary slowly beyond x_α . An inspection of the results of reference 8 shows that the velocity u_m decreases almost linearly with distance x beyond the lift-off point. Therefore, for purposes of integration, it is convenient to replace the cumbersome equation (1) by the simple linear form

$$u_m = u_\alpha - (u_\alpha - 1) \frac{x - x_\alpha}{x_1 - x_\alpha} \quad (40)$$

Utilizing Eqs. (3) and (4) for ΔT_m and y_2 we may write the integrated form of the buoyancy equation to order ΔT_m^2 in the form

$$\phi V = \phi_\alpha V_\alpha + 2g\rho_a y_o^2 c \frac{\Delta T_m}{1+m} \left[I - I_\alpha - \frac{\Delta T_o}{1+m} (J - J_\alpha) \right] \quad (41)$$

where

$$I - I_\alpha = \int_{x_\alpha}^x x v^2 dx \quad (42)$$

$$J - J_\alpha = \int_{x_\alpha}^x x \left(\frac{v^2}{2} + \frac{3v}{4} - \frac{1}{4v} \right) dx \quad (43)$$

Numerical checks show that the J integral contributes very little to the vertical velocity V and will therefore be neglected. The I integral is easily evaluated to yield

$$I - I_\alpha = (x_1 - x_\alpha)^2 \left[\frac{\beta^2}{2} t^2 - 2\beta(u_\alpha - 1) \frac{t^3}{3} + (u_\alpha - 1)^2 \frac{t^4}{4} \right] \Bigg|_{t_\alpha}^t \quad (44)$$

where

$$\beta = u_{\alpha} + 1 + (u_{\alpha} - 1) t_{\alpha} \quad (45)$$

$$t = \frac{x}{x_1 - x_{\alpha}} \quad (46)$$

Making use of Eq. (34) for ϕ , we may write the vertical velocity equation in the form

$$\frac{V}{u_0} = \frac{x_{\alpha}}{x} \frac{(v_{\alpha}^2 - 1)}{v^2 - 1} \frac{f_{\alpha}}{f} \frac{V_{\alpha}}{u_0} + \frac{1}{K} \frac{m}{1+m} \frac{1}{v^2 - 1} \frac{1}{x} (I - I_{\alpha}) \quad (47)$$

where

$$K = \frac{u_0^2}{y_0 g \Delta T_0} \quad (48)$$

is the Froude number for the flow, and f is the value of $a_1 \rho_m$ in Eq. (34), and given to first order in $\Delta T_0 / (1+m)$ by (see Eqs. (9) and (11))

$$f = 1 - \frac{1+v}{2} \frac{\Delta T_0}{1+m} \quad (49)$$

If we employ Eq. (41) for the vertical velocity, the integrated form of the trajectory Eq. (35) may be written as

$$y = \phi_{\alpha} V_{\alpha} \int_{x_{\alpha}}^x \frac{dx}{P} + 2 g \rho_a y_0^2 c \frac{\Delta T_0}{1+m} \left(\int_{x_{\alpha}}^x \frac{I dx}{P} - I_{\alpha} \int_{x_{\alpha}}^x \frac{dx}{P} \right) \quad (50)$$

Using Eq. (39) for P , the integrals in Eq. (50) are easily evaluated to yield

$$y = \frac{x_{\alpha} (v_{\alpha}^2 - 1)}{v(v - 1)} (K_0 - K_1) + \frac{1}{K} \frac{m^2}{1+m} (K_2 - K_1) - \frac{1}{K} \frac{m^2}{1+m} I_{\alpha} (K_0 - K_1) \quad (51)$$

where

$$K_0 = \frac{1}{\beta - 1} \int_{t_\alpha}^t \frac{dt}{t(v-1)} = \frac{1}{\beta - 1} \ln \left(\frac{t}{v-1} \right) \Bigg|_{t_\alpha}^t \quad (52)$$

$$K_1 = \frac{1}{\beta} \int_{t_\alpha}^t \frac{dt}{t v} = \frac{1}{\beta} \ln \left(\frac{t}{v} \right) \Bigg|_{t_\alpha}^t \quad (53)$$

$$K_2 = \int_{t_\alpha}^t \frac{I dt}{t(v-1)}$$

$$K_2 = \left[\frac{(\beta - 1)}{(v_\alpha - 2)^2} a_2 \ln \left(\frac{1}{v-1} \right) - \frac{a_2}{v_\alpha - 2} t + \frac{5\beta + 3}{24} t^2 - \frac{(v_\alpha - 2)}{12} t^3 \right] \Bigg|_{t_\alpha}^t \quad (54)$$

$$K_3 = \int_{t_\alpha}^t \frac{I dt}{t v}$$

$$K_3 = \left[\frac{\beta^3}{12(v_\alpha - 2)^2} \ln \frac{1}{v} - \frac{\beta^2}{12(v_\alpha - 2)} t + \frac{5\beta}{12} t^2 - \frac{(v_\alpha - 2)}{12} t^3 \right] \Bigg|_{t_\alpha}^t \quad (55)$$

$$a_2 = \frac{\beta^2}{2} - \frac{(5\beta + 3)(\beta - 1)}{12} \quad (56)$$

and we have neglected the small term in $\Delta T_0 / (1 + m)$ contributed by f .

3.4 Dependence of Vertical Velocity and Trajectory Upon Parameters

The foregoing results give the general dependence of the vertical velocity and trajectory upon the jet parameters and position. Thus, from Eq. (47) the vertical velocity is proportional to $1/K$ while Eq. (51) indicates the trajectory y is proportional to m/K . This explicit dependence upon m is due to the separation of m and x in the velocity Eq. (1). It is not present in the trajectory for a coflowing jet³ where the dependence of vertical velocity upon windspeed is far more complex.

An examination of Eqs. (47) and (51) shows that the dependence of V/u_0 and y upon position x is more complex than a simple power law. However, an analysis

of numerical solutions of these equations indicates that, roughly, the vertical velocity increases less rapidly than x^2 while the trajectory rises more rapidly than x^2 . These appears to be reasonable results when compared to the coflowing case where $V/u_0 \sim x$, $y \sim x^{5/2}$.

3.5 Scaling Law for Counterflowing Jet

The foregoing results may be utilized to derive the scaling law for a counterflowing jet. An examination of Eqs. (1) and (2) show that, for constant m , the velocity and temperature distributions are independent of length scale. The right hand side of the trajectory Eq. (35) will, therefore, depend only on the Froude number K during a change of scale at constant m (note that the velocity dependence $v^2 \sim T_0^{-1}$ in both numerator and denominator leads to a weak dependence upon T_0 which may be neglected here). This scaling law is in conformity with that obtained for the coflowing jet³ where it is shown that the trajectory depends principally upon the Froude number, the effect of initial temperature T_0 being negligible.

4. ANALYSIS FOR ZONE II

4.1 Axial Distributions

As indicated previously, the axial velocity and temperature in Zone II do not have a large variation and may be obtained by interpolation. Since u_m has the value unity at x_1 and zero at the end of Zone II we write

$$u_m = 1 - S \quad (57)$$

where

$$S = \frac{x - x_1}{x_2 - x_1} \quad (58)$$

and x_2 designates the end of Zone II. The experimental data indicates that Eq. (3) for ΔT_m is fairly accurate in Zone II and will, therefore, be retained in this region.

The surface $y_2(x)$ decreases to zero with a vertical tangent at x_2 ; accordingly, we shall utilize the simple parabolic form

$$y_2 = y_{21}(1 - S)^{1/2} \quad (59)$$

where y_{21} designates the value of y_2 at x_1 .

The experimental data of Vulis¹⁰ indicate that y_3 is roughly constant until y_2 and u_m have decreased to zero. A short distance further out ambient conditions have been attained. For simplicity we shall, therefore, assume y_3 is constant and take the end of Zone II, x_2 , as the termination of the jet, that is, the location at which the jet reverses its direction. Accordingly, we may now write

$$y_3 = y_{31} = y_{21} N_1 \quad (60)$$

where y_{31} , and N_1 are the values of y_3 and N at x_1 . From Eqs. (3) and (12), N_1 is given by

$$N_1 - 1 = 5 \left[1 - \frac{\Delta T_o}{1+m} + \frac{3}{2} \frac{\Delta T_o^2}{(1+m)^2} \right] \quad (61)$$

4.2 Determination of the Buoyant Force

The buoyancy at the position x_1 is given by the integrals I_1 and I_2 in Eqs. (24) and (25), but the values of y_2 , y_3 , v and N are now given by the equations of Section 4.1. Accordingly we first write the buoyancy B as

$$B = 2 g \rho_a y_o^2 (B_1 + B_2 + B_3) \quad (62)$$

where

$$B_1 = \frac{1}{2} \frac{\Delta T_o}{1+m} (y_2 v + y_3) \quad (63)$$

$$B_2 = -\frac{1}{3} \frac{\Delta T_o^2}{(1+m)^2} [y_2(v^2 + v) + y_3] \quad (64)$$

$$B_3 = \frac{1}{4} \frac{\Delta T_o^3}{(1+m)^3} [y_2(v^3 + v^2 + v) + y_3] \quad (65)$$

and then use (59), (60) and (61) to cast B_1 , B_2 and B_3 into the more explicit form

$$B_1 = \frac{1}{2} \frac{\Delta T_o}{1+m} y_{21} [(2-S)(1-S)^{1/2} + 6] \quad (66)$$

10. Abramovich, G. N. (1963) The Theory of Turbulent Jets, The MIT Press, Cambridge, Mass., Chapter 1, pp 32-36.

$$B_2 = -\frac{1}{3} \frac{\Delta T_o^2}{(1+m)^2} y_{21} \left\{ [(2-S)^2 + (2-S)](1-S)^{1/2} + \frac{27}{2} \right\} \quad (67)$$

$$B_3 = \frac{1}{4} \frac{\Delta T_o^3}{(1+m)^3} y_{21} \left\{ [(2-S)^3 + (2-S)^2 + (2-S)](1-S)^{1/2} + \frac{83}{3} \right\} \quad (68)$$

4.3 Calculation of the Trajectory

The flux ϕ in Zone II is, from Eqs. (32) and (33) now given by

$$\phi = \mu_1 + \mu_2 + \mu_3 \quad (69)$$

$$\mu_1 = \frac{y_2}{2} (v-2) + \frac{y_3}{2} \quad (70)$$

$$\mu_2 = \frac{-\Delta T_o}{4(1+m)} [y_2(v^2-2) + y_3] \quad (71)$$

$$\mu_3 = \frac{\Delta T_o^2}{4(1+m)^2} \{y_2[(v-1)(v^2+1)-1]\} \quad (72)$$

while the momentum P is, with Eqs. (37) and (38), now defined by

$$P = \lambda_1 + \lambda_2 + \lambda_3 \quad (73)$$

$$\lambda_1 = \frac{1}{3} y_2 [(v-1)^2 - 1] + \frac{y_3}{2} \quad (74)$$

$$\lambda_2 = \frac{-\Delta T_o}{6(1+m)} \{y_2[(v-1)^2(v+1)-1] + y_3\} \quad (75)$$

$$\lambda_3 = \frac{\Delta T_o^2}{6(1+m)^2} \{y_2[(v-1)^2(v^2+1)-1] + y_3\} \quad (76)$$

Using Section 4.1, we can develop the flux and momentum equations to the form

$$\mu_1 = \frac{y_{21}}{2} [6 - S(1 - S)^{1/2}] \quad (77)$$

$$\mu_2 = \frac{-y_{21}}{2} \frac{\Delta T_o}{1+m} \{[(1 - S)(3 - S) - 1](1 - S)^{1/2} + 16\} \quad (78)$$

$$\mu_3 = \frac{y_{21}}{2} \frac{\Delta T_o^2}{(1+m)^2} \{[(1 - S)(2 - S)^2 - S](1 - S)^{1/2} + 26\} \quad (79)$$

$$\lambda_1 = \frac{y_{21}}{3} \{[(1 - S)^2 - 1](1 - S)^{1/2} + 6\} \quad (80)$$

$$\lambda_2 = \frac{-y_{21}}{6} \frac{\Delta T_o}{1+m} \{[(1 - S)^2(3 - S) - 1](1 - S)^{1/2} + 16\} \quad (81)$$

$$\lambda_3 = \frac{y_{21}}{6} \frac{\Delta T_o^2}{(1+m)^2} \{[(1 - S)^2(2 - S)^2 + (1 - S)^2 - 1](1 - S)^{1/2} + 26\} \quad (82)$$

Because of the dominant effect of the y_3 term, the flux and momentum terms vary very little in the Zone II region. We shall, therefore, utilize average values of these quantities in calculating the vertical velocity and trajectory. Integration of the buoyancy equation now yields for the vertical velocity

$$\frac{V}{u_o} = \frac{6}{\mu} \frac{V_1}{u_o} + (x_2 - x_1) \frac{1}{K} \frac{m}{1+m} \frac{2}{\mu} L \quad (83)$$

where

$$L = \frac{1 - r^{3/2}}{3} + \frac{1 - r^{5/2}}{5} + 3(1 - r) \quad (84)$$

$$\mu = 6 - S(1 - S)^{1/2} \quad (85)$$

$$r = 1 - S \quad (86)$$

in which we have neglected the small contribution of the ΔT_o terms.

Integration of the trajectory equation yields

$$y = y_1 + \frac{3}{2} m \frac{V_1}{u_0} \frac{6}{\lambda} (x - x_1) + \frac{m^2}{1+m} \frac{1}{K} \frac{3}{\lambda} (x_2 - x_1)^2 M \quad (87)$$

$$M = \frac{53}{15} S - \frac{2}{15} (1 - r^{5/2}) - \frac{2}{35} (1 - r^{7/2}) - \frac{3}{2} (1 - r^2) \quad (88)$$

$$\lambda = 6 + [(1 - S)^2 - 1] (1 - S)^{1/2} \quad (89)$$

5. CALCULATION OF UPPER PORTION OF TRAJECTORY

The calculated results show that the slope of the trajectory at the end of Zone I, x_1 , is generally near unity and increasing rapidly as it moves toward a vertical position at x_2 . During this interval the character of the motion has altered from one in which the change of direction is due principally to buoyancy, to one in which it stems primarily from deflection due to wind pressure. The jet velocity drops off more slowly during this interval than during the buoyancy dominated motion. To evaluate the jet velocity at x_2 , we make use of the constancy of momentum in the direction normal to the jet axis,¹¹ that is,

$$\rho_1 u_{m1}^2 \delta_1 \sin \alpha_1 = \rho_2 u_{m2}^2 \delta_2 \sin \alpha_2 \quad (90)$$

where δ is the jet width and α is the angle between the jet velocity and the wind. Since the jet is thoroughly mixed, the densities ρ_1 and ρ_2 may be taken as equal. The mixing coefficient c is more complex here than in the case of a horizontal jet since the angle between the wind and jet directions is no longer constant. For simplicity, we shall — following Abramovich — assume that the value of c is the same as for a horizontal jet. The value of δ_2 is then easily calculated. A numerical check of Eq. (90) for many tests show that u_{m2}^2 is close to $1/2$ of u_{m1}^2 and, for convenience, we shall use the value $1/2$.

As the vertical jet interact with the wind, it is gradually bent over toward a horizontal direction. To obtain this upper trajectory, we employ the method developed by Shandorov for obtaining the path of a jet in a deflecting flow.¹² On the

-
11. Abramovich, G. N. (1963) The Theory of Turbulent Jets, The MIT Press, Cambridge, Mass., Chapter 12, pp 547-548.
 12. Abramovich, G. N. (1963) The Theory of Turbulent Jets, The MIT Press, Cambridge, Mass., Chapter 12, pp 541-556.

basis of many experiments, Shandorov gives an empirical equation which, for the case of wind perpendicular to the jet, may be written as

$$\frac{(x_2 - x)}{2\delta} = \left(\frac{y_e - y}{2\delta} \right)^{2.55} \frac{1}{\rho_e} \frac{1}{u_e^2} \quad (91)$$

where u_e is the initial jet velocity, assumed uniform across the jet, ρ_e the jet density, and y_e the initial vertical coordinate, at the position x_2 . Since the jet is well mixed with air, we may take ρ_e as unity. We shall assume that the velocity profile is linear at x_2 and, therefore, calculate the effective value of u_e by

$$u_e^2 = \frac{1}{3} u_{m2}^2 \quad (92)$$

where u_{m2}^2 is taken as 0.5.

6. DETERMINATION OF LIFT-OFF POINT AND LENGTH OF JET FROM EXPERIMENTAL DATA

In correlating the lift-off point x_α against the experimental data, we shall assume that x_α is proportional to the product of the initial jet velocity u_o and the relative velocity $u_a(m+1)$ and inversely proportional to the temperature excess ΔT_m and write

$$x_\alpha \sim \frac{u_o u_a(m+1)}{g y_o \Delta T_m} \quad (93)$$

Using Eq. (3) for the temperature excess ΔT_m , and noting that m is large compared to unity, Eq. (93) becomes

$$x_\alpha \sim m^2 K \quad (94)$$

where K is the Froude number for the initial flow. Other powers of the initial and relative velocities may be tried in Eq. (93), leading to different combinations of m and K in Eq. (94). However, the relation given by Eq. (94) appeared to yield the best results.

The results of the correlation are shown in Figure 2 where we have plotted the experimental values of the lift-off point x_α against the parameter $p = m K^{1/2}$.

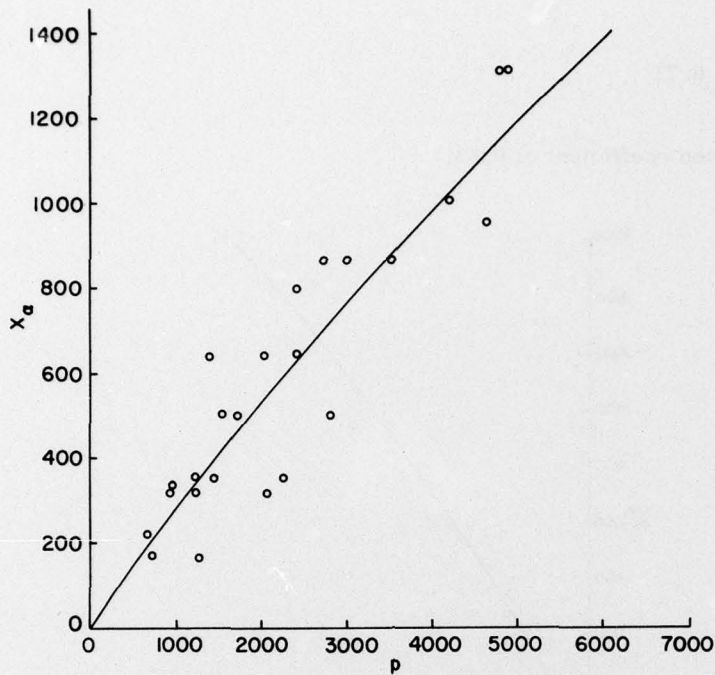


Figure 2. Plot of Experimental Values of Lift-Off Point x_{α} Against Parameter p ; Solid Curve is Power Law Fit to Experimental Points

A fair correlation is obtained, but not as good as that obtained for the coflowing jet. The data has been fitted with a power law curve with the result,

$$x_{\alpha} = 0.66 p^{0.88} \quad (95)$$

and a correlation coefficient of 0.79.

Although the jet length x_2 may be calculated from the model, as shown in reference 8, it is desirable to be able to obtain x_2 from the parameters of the experiment. Since the jet is buoyant, it should depend upon the same parameter used in determining the lift-off point. In addition, in view of the initial heating of the jet, x_2 should drop off inversely to the inlet jet temperature T_0 . However, the use of T_0 in the correlation did not result in any visible improvement of the results. We have, therefore – for convenience – utilized the same parameter p for jet length as previously used for lift-off point. The results of the correlation are shown in Figure 3 where x_2 is plotted against p . The amount of scatter is about the same as that obtained for x_{α} . A power law curve has been fitted to the data yielding

$$x_2 = 4.02 p^{0.71}$$

(96)

with a correlation coefficient of 0.83.

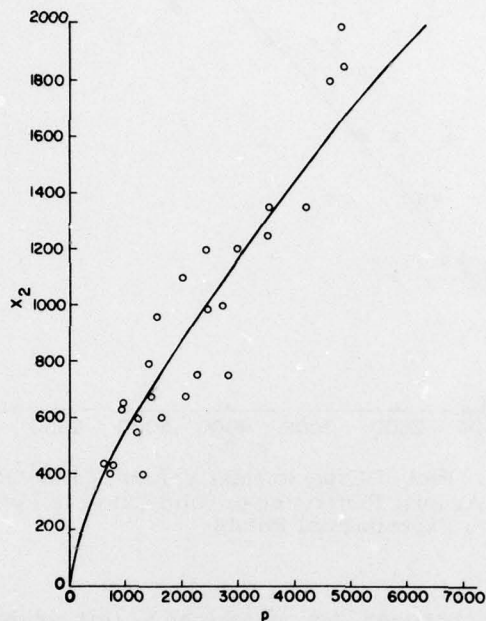


Figure 3. Plot of Experimental Values of Jet Length x_2 Against Parameter p ; Solid Curve is Power Law Fit to Experimental Points

7. RESULTS AND DISCUSSION

The calculated trajectories are shown in Figures 4-9 along with the corresponding experimental curves. These results cover most of the range of windspeeds, initial jet velocities, and initial jet temperatures encountered in the tests. The calculated results are in fair agreement with the experimental curves, but the lower portion of the calculated trajectory generally tends to be somewhat higher than the corresponding experimental result. The lower buoyancy observed experimentally may be due to the fact that when the jets merge, the assumed equivalent planar jet contains regions of cooler air between the jets which help lower the total buoyant force of the jet. In addition, when the jet detaches from the ground some jet air may become entrained with the ambient air going under the jet, resulting in

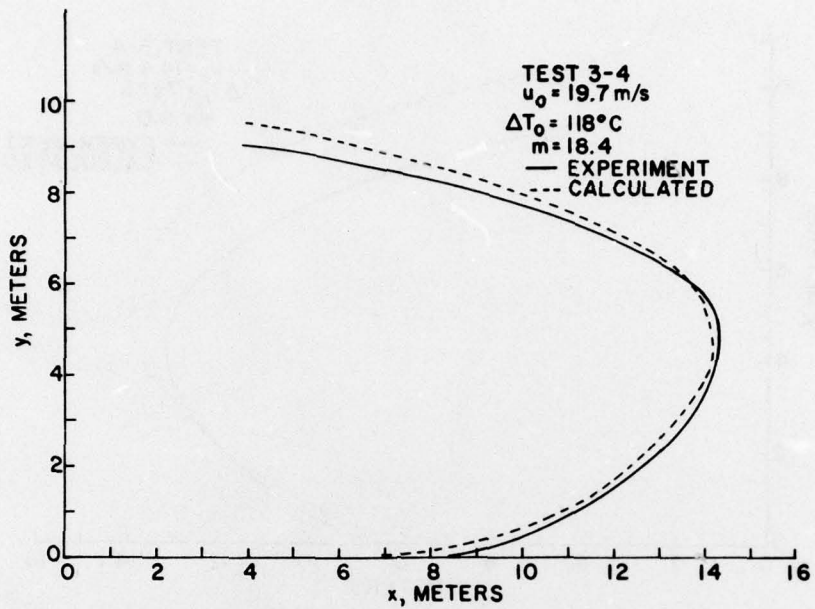


Figure 4. Comparison of Calculated Trajectories, for Several Tests, with Corresponding Experimental Curves, Test 3-4

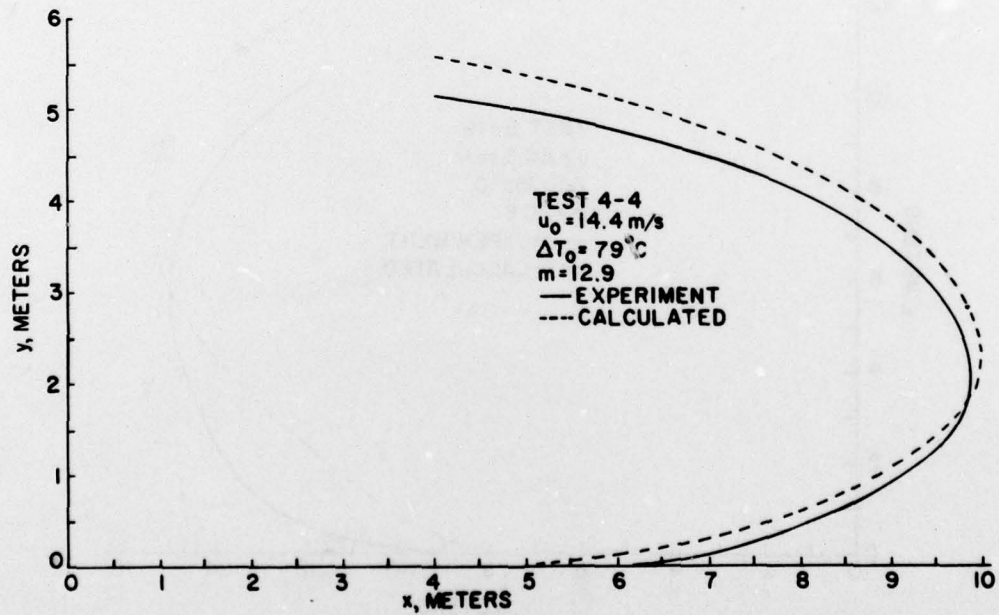


Figure 5. Comparison of Calculated Trajectories, for Several Tests, with Corresponding Experimental Curves, Test 4-4

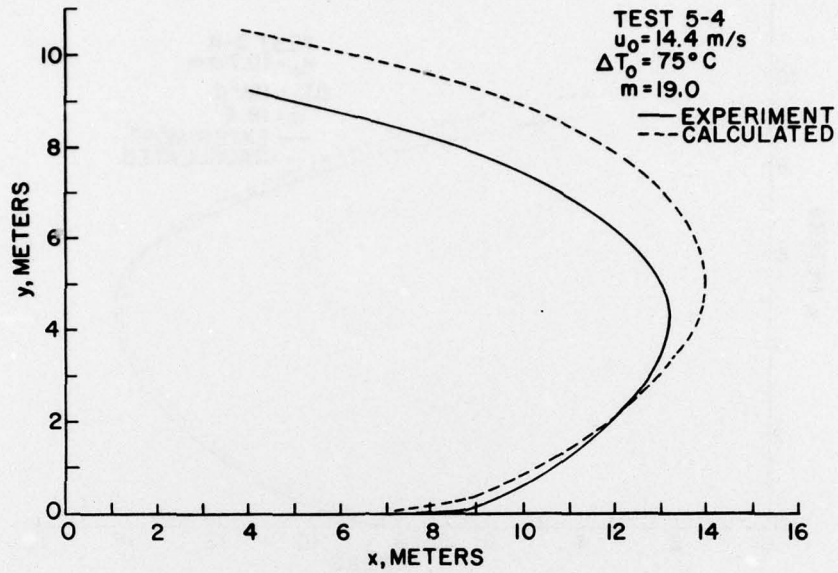


Figure 6. Comparison of Calculated Trajectories, for Several Tests, with Corresponding Experimental Curves, Test 5-4

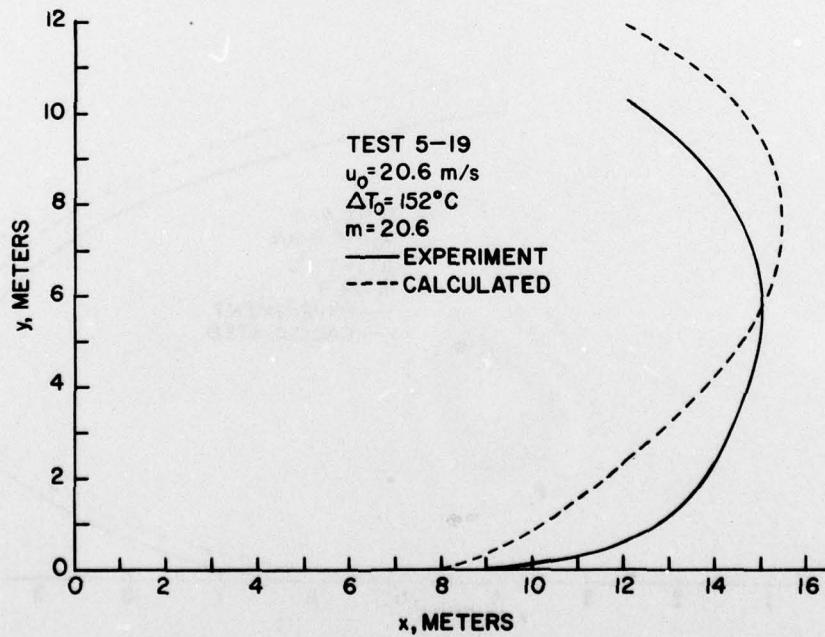


Figure 7. Comparison of Calculated Trajectories, for Several Tests, with Corresponding Experimental Curves, Test 5-19

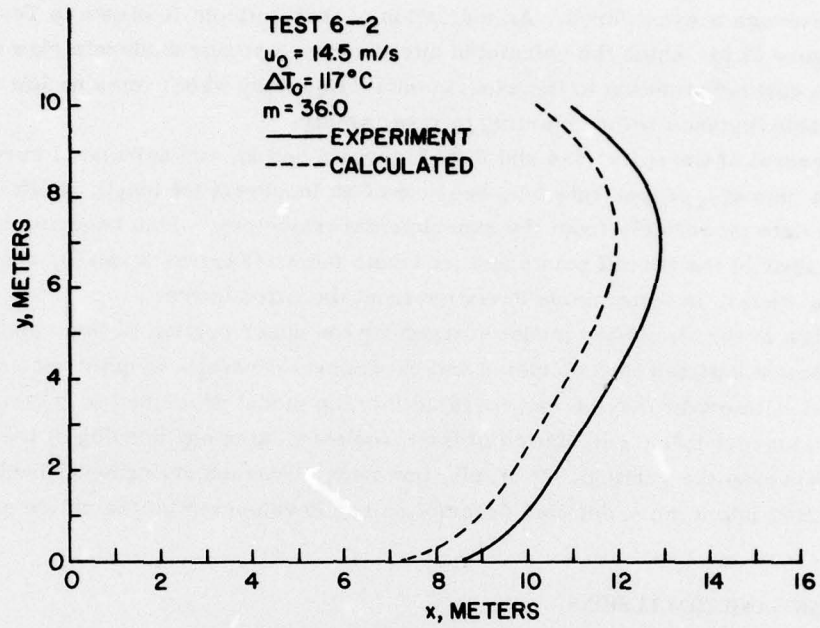


Figure 8. Comparison of Calculated Trajectories, for Several Tests, with Corresponding Experimental Curves, Test 6-2

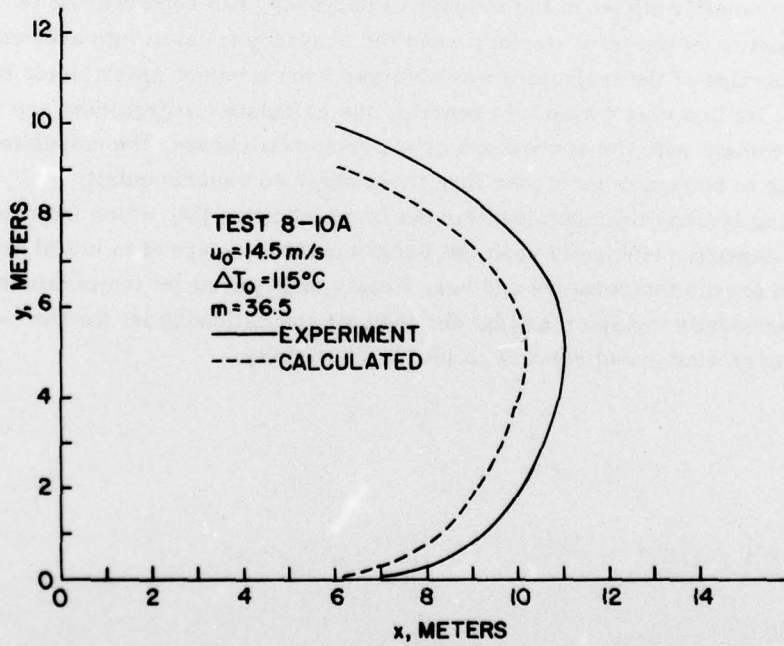


Figure 9. Comparison of Calculated Trajectories, for Several Tests, with Corresponding Experimental Curves, Test 8-10A

lower average buoyant force. An indication of these effects is shown in Test 5-19 (Figure 7) for which the calculated curve shows a steady moderate rise after lift-off in contradistinction to the experimental trajectory which remains low a considerable distance before starting to rise rapidly.

In several of the tests, 5-4 and 6-2 (Figures 6 and 8), the calculated curves appear to rise at a proper rate but, because of an incorrect jet length or lift-off point, deviate moderately from the experimental trajectory. This behavior is due to the scatter of the lift-off points and jet length points (Figures 2 and 3), resulting, in several cases, in appreciable deviation from the fitted curves.

In view of the simplified model utilized for the upper portion of the trajectory, the agreement between the calculated and experimental results is quite reasonable. Additional refinement may be incorporated into the model described in Section 5, that is, a more detailed calculation of the turbulent mixing and bending of the curve as it approaches the vertical. It is felt, however, that such refinement should be incorporated into a more detailed description and development of the entire model.

8. SUMMARY AND CONCLUSIONS

A model, previously developed for obtaining the dynamic properties of a heated turbulent counterflowing jet in the absence of buoyancy, has been utilized to obtain the lower portion of the jet trajectory when the buoyancy is taken into account. The upper portion of the trajectory was obtained from a model which yields the deflection of a jet in a cross wind. In general, the calculated trajectories are in fair to good agreement with the corresponding experimental curves, the calculated results tending to be somewhat higher than those obtained experimentally.

A scaling law has been obtained for the counterflowing jet, which indicates that the scaling depends principally upon the Froude number referred to initial jet velocity and excess temperature and very weakly upon initial jet temperature. This result is essentially the same as that obtained for the coflowing jet for the case of small values of wind speed relative to initial jet velocity.

References

1. Abramovich, G. N. (1963) The Theory of Turbulent Jets, The MIT Press, Cambridge, Mass., Chapters 4 and 9.
2. Abramovich, G. N. (1963) The Theory of Turbulent Jets, The MIT Press, Cambridge, Mass., Chapter 12, pp 580-585.
3. Klein, M. M., and Kunkel, B. A. (1975) Interaction of a Buoyant Turbulent Planar Jet With a Coflowing Wind, AFCRL-TR-75-0368.
4. Klein, M. M., and Kunkel, B. A. (1975) Interaction of a Buoyant Turbulent Round Jet With a Coflowing Wind, AFCRL-TR-75-0581.
5. Klein, M. M. (1977) A Method for Determining the Point of Lift-Off and Modified Trajectory of a Ground-Based Heated Turbulent Planar Jet in a Coflowing Wind, AFGL-TR-77-0033.
6. Abramovich, G. N. (1963) The Theory of Turbulent Jets, The MIT Press, Cambridge, Mass., Chapter 4.
7. Sekundov, A. N. (1969) The Propagation of a Turbulent Jet in an Opposing Stream, in Turbulent Jets of Air, Plasma and Real Gas, Consultants Bureau, New York.
8. Klein, M. M. (1977) Interaction of a Turbulent Planar Heated Jet With a Counterflowing Wind, AFGL-TR-77-0214.
9. Kunkel, B. A. (1975) Heat and Thrust Requirements of a Thermal Fog Dispersal System, AFCRL-TR-75-0472.
10. Abramovich, G. N. (1963) The Theory of Turbulent Jets, The MIT Press, Cambridge, Mass., Chapter 1, pp 32-36.
11. Abramovich, G. N. (1963) The Theory of Turbulent Jets, The MIT Press, Cambridge, Mass., Chapter 12, pp 547-548.
12. Abramovich, G. N. (1963) The Theory of Turbulent Jets, The MIT Press, Cambridge, Mass., Chapter 12, pp 541-556.

List of Symbols

b	distance from outside wall to jet axis
c	jet thickness coefficient
H	end of initial section
K	Froude number
m	wind speed parameter = u_o/u_a
p	jet parameter = $mK^{1/2}$
T	jet temperature
T_a	ambient temperature
T_m	temperature on axis
ΔT	temperature excess over ambient ($T - T_a$)
u	jet velocity
u_m	velocity on axis
V	vertical velocity
x	horizontal position along jet
x_H	end of initial section
x_1	end of Zone I
x_2	end of Zone II

x_α lift-off position
 y vertical position
 y_0 jet half-width
 y_2 zero velocity surface in main section
 y_3 surface separating perturbed and unperturbed flows
 α angle between jet and wind
 ρ gas density
 δ jet width

Subscripts

a ambient
c region above y_3 surface
m on jet axis
o initial jet position
 α lift-off position
e initial position